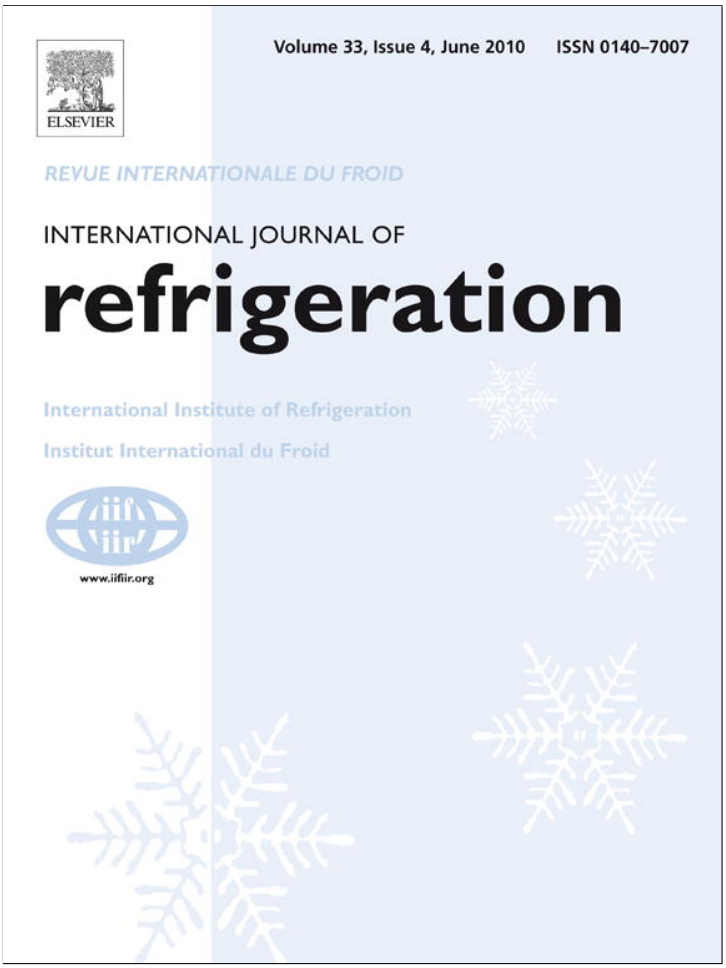

INTERNATIONAL JOURNAL OF REFRIGERATION 33 (2010) 765–773

available at www.sciencedirect.com

ScienceDirect

journal homepage: www.elsevier.com/locate/ijrefrig

An air-standard cycle and a thermodynamic perspective on operational limits of Ranque–Hilsh or vortex tubes

*José Roberto Simões-Moreira**

SISEA – Alternative Energy Systems Laboratory in the Mechl. Eng. Department at Escola Politécnica, Post-Graduation Program on Energy at Institute of Electrotechnical and Energy, University of São Paulo, Av. Prof. Mello Moraes, 2231, 05508-900, São Paulo, SP, Brazil

ARTICLE INFO

Article history:
Received 18 October 2009
Received in revised form
8 January 2010
Accepted 20 January 2010
Available online 1 February 2010

Keywords:
Vortex tube
Thermodynamic cycle
Ranque-Hilsch
Energy balance
COP

ABSTRACT

A Thermodynamic air-standard cycle was envisaged for Ranque–Hilsh (R–H) or Vortex Tubes to provide relevant Thermodynamic analysis and tools for setting operating limits according to the conservation laws of mass and energy, as well as the constraint of the Second Law of Thermodynamics. The study used an integral or control volume approach and resulted in establishing working equations for evaluating the performance of an R–H tube. The work proved that the coefficient of performance does not depend on the R–H tube operating mode, i.e., the same value is obtained independently if the R–H tube operates either as a heat pump or as a refrigeration device. It was also shown that the isentropic coefficient of performance displays optima values of cold and hot mass fractions for a given operating pressure ratio. Finally, the study was concluded by comparing the present analysis with some experimental data available in the literature for operating pressures ranging 2–11 atm.

Cycle à air traditionnel, aspects thermodynamiques et limites du fonctionnement des tubes Ranque-Hilsch ou vortex

Mots clés : Tube vortex ; Cycle thermodynamique ; Ranque-Hilsch ; Bilan énergétique ; COP

1. Introduction

Thermal energy separation phenomenon in Ranque–Hilsh or vortex tubes, or R–H tube for short, was first observed by Ranque (1933) when he was carrying out some experiments with a so called vortex pump. Later, shortly after World War II, Hilsch (1946) brought the device to scientific discussion by showing its cooling capability.

Ranque found that by injecting a compressed air stream tangentially and perpendicularly to a simple hollow cylinder open at both ends that two swirling flow streams developed inside the tube moving toward to the tube ends. At regions near the wall it was noticed a high velocity flow having an average temperature superior to that one of the intake air stream. Near the tube centerline, a jet flew out throughout the tube at a lower temperature. Hilsch intensely explored the

* Tel./fax: +55 11 30915684.
E-mail addresses: jrsimoes@usp.br, jose.moreira@poli.usp.br (J.R. Simões-Moreira).
0140-7007/$ – see front matter © 2010 Elsevier Ltd and IIR. All rights reserved.
doi:10.1016/j.ijrefrig.2010.01.005

Nomenclature

COP	coefficient of performance [-]
COP_{HP}	heat pump – coefficient of performance [-]
COP_R	refrigeration - coefficient of performance [-]
COP_S	isentropic or ideal – coefficient of performance [-]
C_V	constant heat capacity at constant volume [kJkg^{-1}K^{-1}]
C_P	constant heat capacity at constant pressure [kJkg^{-1}K^{-1}]
h	specific enthalpy [kJkg^{-1}]
k	ratio between heat capacities [-]
$\dot{m}$	mass flux [kgs^{-1}]
P	pressure [kPa]
P_{atm}	atmospheric pressure [kPa]
$\dot{Q}$	cooling or heating load [kW]
R	gas constant [kJkg^{-1}K^{-1}]
R_P	pressure ratio [-]
s	specific entropy [kJkg^{-1} K^{-1}]
T	absolute temperature [K]
$\dot{W}$	total compression power [kW]

Greek

Δ	variation [-]
θ	dimensionless temperature [-]
μ	mass fraction [-]

Subscripts

atm	atmosphere
0	air inlet flow
H	air hot exit flow
L	air cold exit flow

Superscripts

*	optimal operating condition

apparatus and proposed the first tentative theory to explain the thermal energy separation. R–H tubes are also known as ''vortex tubes'' and the first term will be used through out this paper because of its historical reasons. Some authors also prefer to name the device as ''Ranque–Hilsh Vortex Tube'', or simply RHVT.

Effort has been devoted to understand the fluid dynamics and the energy separation physics for determining the fundamental operation principle of this puzzling device. Since Hilsh brought up the device to discussion, many researchers have been working on the problem in order to understand on how it operates and what the dominating physical phenomena behind the tube are. There were quite some interest and research activities on R–H tubes in the 50s and 60s. One can mention the experimental and analytical work carried out by Fulton (1950); Scheper (1951); Pengelley (1957); Hartnett and Eckert (1957); Martynovskii and Alekseev (1957); Lay (1959); Deissler and Perlmutter (1960); Metenin (1961); Reynolds (1964), and Takahama (1965), among others. More recent papers on the subject are Lewins and Bejan (1999); Ahlborn and Gordon (2000); Saidi and Valipour (2003); Behera et al. (2005); Aljuwayhel et al. (2005); Gao et al. (2005); Dincer et al. (2008); Nimbalkar and Muller (2009), among others. The literature is quite extensive and it is not the goal of this paper to make a thorough review on R–H tubes and the reader is directed to the recent paper of Eiamsa-ard and Promvonge (2008) for a comprehensive review.

Presently, R–H tubes have been widely used in applications such as cooling devices and heat pumps, simply by their characteristic of separating the compressed inflow air into cold and hot flows and directing them to the desired application. Other less conventional applications are particle and gas separation or gas cleaning besides many other versatile applications as revised by Khodorkov et al. (2003).

Constructively there are two types of R–H tubes: the counter flow one, developed and studied by Ranque and Hilsh, which still continues to be extensively investigated nowadays; and the uni-flow R–H tube, in which the two air flows exit in the same side of the tube end. According to Eiamsa-ard and Promvonge (2008), much of the recent experimental investigations of vortex tubes have been divided into two main categories: (1) parametric studies, which aims at varying geometrical parameters of the vortex tube components and to observe their effects on the tube performance; (2) studies focused on the mechanism of energy separation and flow inside the R–H tube by measuring pressure, velocity, and temperature profiles at various stations between the inlet nozzle and the exits. The effective parameters that control the temperature separation can be separated further into two groups, the geometrical and thermo-physical parameters. Most of the experimental studies made on vortex tubes are related to small internal diameter. Eiasma-ard and Promvonge comment that most of the R–H tubes investigated in their work have internal diameter less than 10 mm, generally used for laboratory investigations and for cooling finalities.

Internal processes that generate the two different air streams are the central unanswered question. Although numerous efforts, theories and hypotheses have been formulated in order to elucidate the dominating physical mechanisms within the tube, this paper will address the question from a broader point-of-view using an integral or control volume approach based on the application of the laws of conservation of mass and energy as well as the Second Law of Thermodynamics. Firstly, it will be proposed a Thermodynamic air-standard cycle in a very similar fashion to any other air-standard cycles such as the air refrigeration cycle, Otto, Diesel, and Brayton, to name a few. As usual, the main simplification of the ideal gas behavior with constant heat capacities will lead the analysis to ideal working equations, including a proper definition of a COP – coefficient of performance – of the air-standard Ranque–Hilsh Thermodynamic cycle. The study shows that the COP is the same independently if a R–H tube works either as a heat pump or as a refrigeration device. Secondly, the paper will analyze the

constraints imposed by the Second Law of Thermodynamics that will result in establishing the limits of operation of any R–H tube. Any R–H tube will operate between the isentropic or ideal condition and the adiabatic throttling process for a given inlet thermodynamic state. Finally, the study will show that an ideal R–H tube has optimal operating conditions for which the *COP* is optimum.

2. R–H tube as an air-standard thermodynamic cycle

In an R–H tube operation compressed air is split into two streams of air, being one colder and the other hotter than the inlet compressed air. Depending on one's interest the piece of equipment can be used as a heat pump, or a refrigeration device, or both. The modeling study initiates by establishing the same fundamental assumptions as those that are made for any air-standard cycle analysis. Basically, the working fluid is air characterized by constant specific heats and its behavior is described by the ideal equation-of-state. By doing so, a simple way to obtain Thermodynamic relationships, operation limits, and performance can be obtained by applying the laws of conservation of mass and energy, as well as the second law. While in actual operation air is released by the two tube exits to atmosphere, for modeling purposes it is necessary to assume that the working fluid undergoes a closed Thermodynamic cycle. Such hypothesis is not completely out of reality if one considers that the two exiting air streams will discharge into an environment (such as the atmosphere) to undergo next some cooling or heating with the surroundings to reach the Thermodynamic equilibrium with the environment once again. At the same time, air will go through an ideal compression process to obtain the compressed air that feeds the R–H tube. Ideally it will be considered that the compression process is a reversible isothermal one. The compression process is a point that can bring some controversy as one may consider an isentropic compression rather than a reversible isothermal one. In favor of the latter one is that the air is usually fed into the tube at the local temperature and if one considers the isentropic compression, an additional heat exchanger after the compressor would be necessary to remove heat from the air as the final air temperature will be above the local one. Also, ideally one may want to have a minimum shaft power consumption for the air compression process, which can only be achieved with a well cooled compressor in order to approach as much as possible the reversible isothermal compressor. Therefore, the ideal compression process is used for establishing the air-standard process is the reversible isothermal one.

Fig. 1 shows a schematic of the conceived air-standard cycle. Constant pressure heating and cooling processes are made by the two heat exchangers mounted downstream the two tube exits and they represent the R–H tube cooling and heating thermal loads capacity, respectively. The cold air stream ($\dot{m}_L$) that leaves the R–H tube is labeled "L" and it will receive the cooling load $\dot{Q}_L$ for the case the R–H tube is in the refrigeration operation mode. Ideally, after receiving the cooling load in a heat exchange constant pressure process the air stream will be heated up to the environment temperature, T_0. On the other hand, the hot air stream ($\dot{m}_H$), labeled "H", leaves the tube at the right tube end and it will deliver the heating load $\dot{Q}_H$ in a constant pressure heat exchange process whenever the R–H tube operates in the heat pump operation mode. Consequently, the hot air stream will be cooled off to reach the environment temperature, T_0. In order to close the circuit the two air streams merge together at T_0 and P_{atm}, to make up again the total mass flux, $\dot{m}_o$. Next, the total air stream at the environmental conditions undergoes a compression process in the ideal isothermal compressor to raise the pressure from the atmospheric condition to the operational pressure, P_0. Finally, once again the compressed air at T_0 and P_0 at the tube inlet will undergo the complex splitting phenomena within the R–H tube to conclude the thermodynamic cycle (Fig. 1).

2.1. The laws of conservation of mass and energy

Using the schematics of Fig. 1, the mass conservation law in steady state applied to the R–H tube can be written as:

$$\dot{m}_0 = \dot{m}_L + \dot{m}_H, \tag{1}$$

which, in terms of mass fractions becomes:

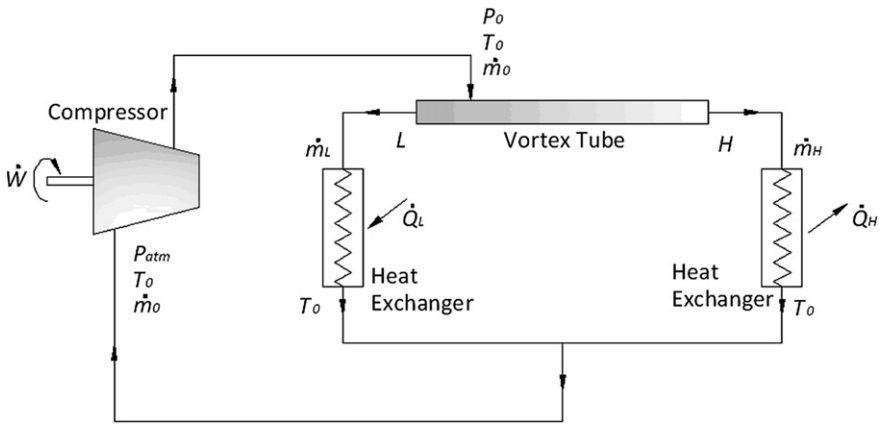

Fig. 1 – Schematics of the air-standard cycle for the R–H tube.

$$\mu_L + \mu_H = 1. \tag{2}$$

where, the cold mass fraction is defined as:

$$\mu_L = \frac{\dot{m}_L}{\dot{m}_0}, \tag{3}$$

whereas, the hot mass fraction is defined as:

$$\mu_H = \frac{\dot{m}_H}{\dot{m}_0}, \tag{4}$$

From the First Law of Thermodynamics in steady state applied to the R–H tube it is possible to write:

$$\dot{m}_0 h_0 = \dot{m}_L h_L + \dot{m}_H h_H \tag{5}$$

All other forms of energy have been neglected, but the specific enthalpy. From the hypothesis of ideal gas with constant heat capacities along with the definitions given by Eqs. (2) and (3), one may obtain the alternative form of the equation of conservation of energy (Eq. (5)):

$$(1-\mu_L)\theta_H + \mu_L\theta_L = 1, \tag{6}$$

where, $\theta_H = T_H/T_0$ and $\theta_L = T_L/T_0$, are the dimensionless hot and cold temperatures, respectively. Alternatively, if one wants to have an equation explicit on hot mass fraction, Eq. (6) can be written as:

$$\mu_H\theta_H + (1-\mu_H)\theta_L = 1, \tag{7}$$

The ideal isothermal compression leads to the following expression for the total compression power:

$$\dot{W} = \dot{m}_0 R T_0 \ln\left(\frac{P_0}{P_{atm}}\right) \tag{8}$$

Cooling, $\dot{Q}_L$, and heating, $\dot{Q}_H$, loads can be obtained by applying the first law of Thermodynamics in steady state separately to the two heat exchanges depicted in Fig. 1. Also, with the ideal behavior hypothesis, one will obtain the following two equations:

$$\dot{Q}_L = \dot{m}_L C_P (T_0 - T_L), \tag{9}$$

and

$$\dot{Q}_H = \dot{m}_H C_P (T_H - T_0). \tag{10}$$

For the refrigeration cycle operation mode as usual the COP_R is given by the ratio between the cooling load and the compression power, i.e.,

$$COP_R = \frac{|\dot{Q}_L|}{\dot{W}}. \tag{11}$$

after substituting Eqs. (3), (8), and (9) along with the ideal gas hypothesis with constant heat capacity at constant pressure, C_P, and constant volume, C_V, one obtains the following working equation:

$$COP_R = \mu_L \frac{k}{k-1}\frac{(1-\theta_L)}{\ln(R_P)}, \tag{12}$$

where, k is the ratio between heat capacities, i.e.,

$$k = \frac{C_P}{C_V}, \tag{13}$$

and the pressure ratio, R_P, is defined by:

$$R_P = \frac{P_0}{P_{atm}}. \tag{14}$$

In the heat pump operation mode, one may define the following expression for the COP_{HP} – coefficient of performance:

$$COP_{HP} = \frac{|\dot{Q}_H|}{\dot{W}} \tag{15}$$

In a similar fashion, after substituting Eqs. (4), (8), and (10) into the above equation one obtains the following working equation for the R–H tube in heat pump operation mode:

$$COP_{HP} = \mu_H \frac{k}{k-1}\frac{(\theta_H - 1)}{\ln(R_P)} \tag{16}$$

2.2. *The second law of thermodynamics constraint*

The Second Law of Thermodynamics limits the steady state operation of an adiabatic Ranque–Hilsh tube by imposing the following constraint over the tube:

$$\dot{m}_L s_L + \dot{m}_H s_H \geq \dot{m}_0 s_0 \tag{17}$$

where the subscripts "0", "L", and "H" apply for the air inlet flow and cold and hot exit flows, as before. After applying the mass conservation equation (Eq. (1)) and the definition of the cold mass flow ratio (Eq. (3)), one may obtain:

$$\frac{(1-\mu_L)}{\mu_L}\Delta s_L + \Delta s_H \geq 0 \tag{18}$$

where, $\Delta s_L = s_L - s_0$ and $\Delta s_H = s_H - s_0$. From the assumed hypotheses, the specific entropy variation can be written as function of pressure and temperature according to:

$$\Delta s_L = C_P \ln\left(\theta_L R_P^{\frac{k-1}{k}}\right) \tag{19}$$

and

$$\Delta s_H = C_P \ln\left(\theta_H R_P^{\frac{k-1}{k}}\right) \tag{20}$$

substituting Eqs. (6), (19), and (20) into Eq. (18), and after rearranging it, one will obtain the following second law constraint:

$$\theta_L^{\mu_L}\left[\frac{1-\mu_L\theta_L}{1-\mu_L}\right]^{(1-\mu_L)} \geq R_P^{\frac{1-k}{k}} \tag{21}$$

the above expression is more suitable for the refrigeration operation mode as it possesses only magnitudes relevant to refrigeration cycle. A second and absolutely equivalent form of the above equation can also be obtained when the R–H is operating as a heat pump where the related magnitudes are explicitly obtained:

$$\theta_H^{\mu_H}\left[\frac{1-\mu_H\theta_H}{1-\mu_H}\right]^{(1-\mu_H)} \geq R_P^{\frac{1-k}{k}} \tag{22}$$

3. Analysis of limits of operation and performance

3.1. *Limits of operation*

The isentropic condition sets the ideal limit of operation. Given a known mass fraction and a pressure ratio, the minimum allowable cold air stream temperature is given by

Eq. (21), whereas Eq. (22) sets the maximum hot air stream temperature. Evidently, the other limit of operation occurs when the R–H tube does not work at all (being an adiabatic throttling device). In this case, the two air stream temperatures will be at the same inlet temperature, and $\theta_L = \theta_H = 1$.

In order to analyze the ideal condition, firstly the inequality sign that appears in Eqs. (21) and (22) must be replaced by the equality sign. Two limits for the mass fractions matter in this case. The first one is the case where the cold mass fraction vanishes, i.e.,$\mu_L \to 0$, which is equivalent to $\mu_H \to 1$. Applying that limiting condition to Eq. (21), one obtains:

$$\lim_{\mu_L \to 0} \frac{\theta_L^{\mu_L}\left[\frac{1-\mu_L\theta_L}{1-\mu_L}\right]^{(1-\mu_L)}}{R_P^{\frac{1-k}{k}}} = 1 \Rightarrow \theta_L = 0, \tag{23a}$$

now, applying the same condition to Eq. (22), one obtains:

$$\lim_{\mu_H \to 1} \frac{\theta_H^{\mu_H}\left[\frac{1-\mu_H\theta_H}{1-\mu_H}\right]^{(1-\mu_H)}}{R_P^{\frac{1-k}{k}}} = 1 \Rightarrow \theta_H = 1, \tag{23b}$$

The other limit occurs when the cold mass fraction approaches the unity, i.e., $\mu_L \to 1$, which is equivalent to $\mu_H \to 0$ (hot mass fraction vanishes). So, carrying out those limits, one obtains:

$$\lim_{\mu_L \to 1} \frac{\theta_L^{\mu_L}\left[\frac{1-\mu_L\theta_L}{1-\mu_L}\right]^{(1-\mu_L)}}{R_P^{\frac{1-k}{k}}} = 1 \Rightarrow \theta_L = R_P^{\frac{1-k}{k}}, \tag{24a}$$

now, applying the same condition to Eq. (23b), one obtains:

$$\lim_{\mu_H \to 0} \frac{\theta_H^{\mu_H}\left[\frac{1-\mu_H\theta_H}{1-\mu_H}\right]^{(1-\mu_H)}}{R_P^{\frac{1-k}{k}}} = 1 \Rightarrow \theta_H \to \infty, \tag{24b}$$

It is noteworthy to mention that the dimensionless cold temperature never can reach the zero value as given by the limit in Eq. (23a). One must take into account that the cold mass fraction is also going simultaneously to zero ($\mu_L \to 0$) and as so, the hot mass fraction approaches the unit ($\mu_H \to 1$) and the dimensionless hot temperature goes to unity as well. In this case the R–H tube will work as an adiabatic throttling device. Being the work fluid an ideal gas with constant heat capacities, the temperature variation is also nil, i.e., $\theta_H = 1$.

The second important observation regarding the above limits is that Eq. (24a) represents the isentropic expansion of the total air mass flow rate ($\mu_L \to 1$) as if it were ideally expanding from P_0 to P_{atm}. Of course, the unbound upper limit for the dimensionless hot temperature has only mathematical significance as the hot mass fraction also vanishes ($\mu_H \to 0$). In this case the R–H will work as an isentropic expansion device and the temperature variation is the isentropic one associated with the expansion, i.e., the limit indicated for θ_L given by Eq. (24a).

Graphs in Figs. (2) and (3) show the dependence of the dimensionless cold and hot temperature with the mass fraction respectively. Concerning the graph in Fig. (2), the lower isentropic limit given by Eq. (21) for θ_L as a function of the cold mass fraction is shown and it is represented by the lower

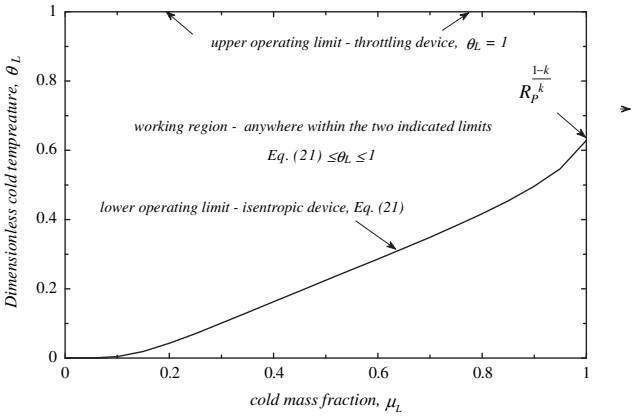

Fig. 2 – Dimensionless cold temperature, θ_L, versus cold mass fraction, μ_L. Pressure ratio, $R_P = 5$, air atmospheric ($k = 1.4$).

curve. The upper limit horizontal straight line (θ_L) represents the case the R–H tube does not operate at all, being a simple adiabatic throttling device without any temperature variation. Actual operating range of an R–H tube falls within those two limits.

In Fig. (3), it is shown the behavior of θ_H as a function of the hot mass fraction. The upper limiting curve corresponds to the isentropic condition given by Eq. (22). As discussed previously, the hot temperature tends to infinity as the hot mass fraction goes to zero. The lower horizontal straight line ($\theta_H = 1$) is valid for the case the R–H tube works as a throttling device without any temperature change. Evidently, any actual operating condition falls within those two limits. It is important to recall that the both graphs of Figs. (2) and (3) do represent the same phenomenon and, therefore, are completely alike. It is a matter of one's choice to decide for which set of independent variables one is willing to work with.

3.2. *Analysis of performance*

The performance analysis of an R–H tube is given by analyzing the overall behavior of the COP as for any other refrigeration

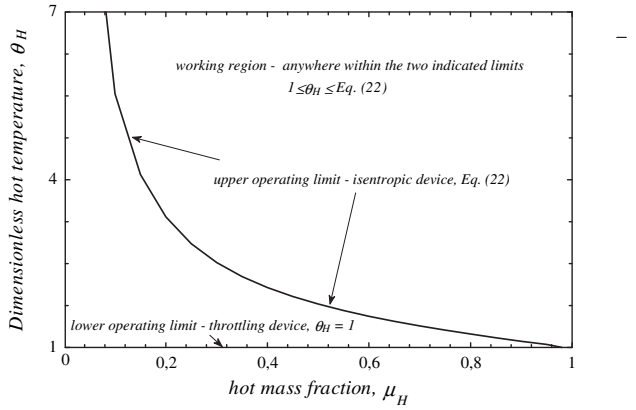

Fig. 3 – Dimensionless hot temperature, θ_H, versus cold mass fraction, μ_H. Pressure ratio, $R_P = 5$, air atmospheric ($k = 1.4$).

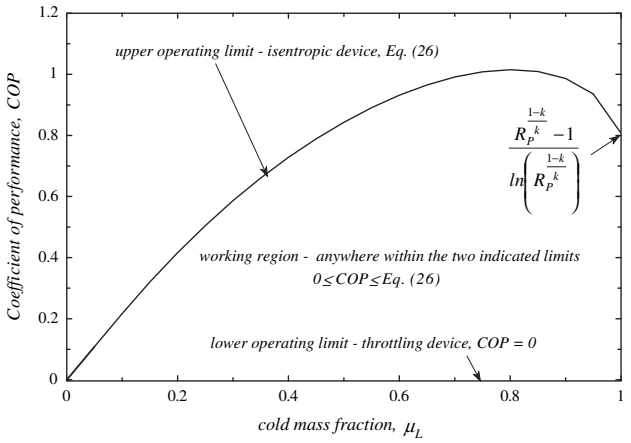

Fig. 4 – Coefficient of performance, COP, versus cold mass fraction, μ_H. Pressure ratio, $R_P = 5$, air atmospheric ($k = 1.4$).

device. Firstly, it is necessary to show that Eqs. (12) and (16) are equal. In order to prove that, first substitute θ_L from Eq. (6) along with the fact that $\mu_L = 1-\mu_H$, as defined by Eq. (2), into Eq. (12). After rearranging it, the twin expression (Eq. (16)) will emerge. Therefore, henceforth it is not necessary to make any distinction between the coefficients of performance of an R–H tube, and the subscripts "R" and "HP" can be dropped off. Therefore:

$$COP = COP_R = COP_{HP} \tag{25}$$

it is quite surprisingly that the COP of an R–H tube does not depend on its operating mode: the COP will always be the same. So, one can say simply say" COP of an R–H tube" without adding any adjective to it.

The second important feature of the R–H tube performance is the behavior of the COP with the mass fraction. The analysis is accomplished as before by establishing the limiting conditions of the COP. The upper COP limit is set for the isentropic behavior of the R–H tube and a subscript "s" will be used to denote it. In order to obtain the isentropic COP_S dependence on the cold mass fraction, let one first isolate θ_L from Eq. (12) and substitute it into Eq. (21) considering the equal sign to obtain:

$$\left(1+\frac{COP_S\times\ln(R_P)^{\frac{1-k}{k}}}{\mu_L}\right)^{\mu_L}\left(1-\frac{COP_S\times\ln(R_P)^{\frac{1-k}{k}}}{1-\mu_L}\right)^{(1-\mu_L)} = R_P^{\frac{1-k}{k}} \tag{26}$$

Notice that the ideal COP_S is implicitly defined by the previous equation. Eq. (26) is best seen in graph form as shown in (Fig. 4), which has been denoted upper operating limit curve. Keeping the COP_s behavior in mind it is useful to determine the minimum and maximum limits for the cold mass fraction. The first limit of Eq. (26) is for the case where the cold mass fraction vanishes, i.e., $\mu_L = 0$, which also leads to $COP_S = 0$. The other limit of Eq. (26) is for the case where $\mu_L \to 0$, which gives the following value:

$$\lim_{\mu_L\to 1} COP_S = \frac{R_P^{\frac{1-k}{k}}-1}{\ln\left(R_P^{\frac{1-k}{k}}\right)} \tag{27}$$

For sake of simplicity, Eq. (26) was not rewritten down. The above limit is shown in the right hand side of the upper curve in Fig. (4).

With the isentropic operation investigated, one may now analyze the situation for which the R–H tube works just as an adiabatic throttling device. In this case the COP will be zero everywhere no matter the cold (or the hot) mass fraction as indicated in Fig. (4) by the lower operating limit straight line. Furthermore, once established both the isentropic and the adiabatic throttling operating situations, it is straightforward to recognize that the actual COP for any R–H tube will fall within the region bordered by the isentropic curve (upper one) and the nil COP as shown in Fig. (4).

Fig. (4) also reveals a remarkable behavior of the COP_s as a function of the cold mass fraction. It displays an optimum or maximum COP_s for a given pressure ratio. As usual the condition of a local maximum is given by:

$$\left.\frac{\partial(COP_S)}{\partial\mu_L}\right)_{R_P} = 0, \tag{28}$$

which, applied to Eq. (26) and after considerable work yields:

$$\mu_L^* = \frac{\theta_L^*\ln\left(\frac{R_P^{\frac{1-k}{k}}}{\theta_L^*}\right)+\theta_L^*-1}{(\theta_L^*)^2\ln\left(\frac{R_P^{\frac{1-k}{k}}}{\theta_L^*}\right)+\theta_L^*-1}, \tag{30}$$

where, the (*) superscript was added to recall that the optimal operating condition set by Eq. (30) is valid only for the isentropic situation where the COP_S is maximum for a given pressure ratio. In order to find the numerical values of the maximum condition conditions, μ_L^* from Eq. (30) should be substituted into Eq. (21) for a given pressure ratio as well as a known heat capacities ratio. Of course, there is an enormous effort to have a simple straight expression. So, rather than doing that, Eq. (21) is rewritten down below as Eq. (31). Then, it is suggested to simultaneously solve both non-linear equations Eqs. (30 and 31) by any suitable numerical method.

$$(\theta_L^*)^{\mu_L^*}\left[\frac{1-\mu_L^*\theta_L^*}{1-\mu_L^*}\right]^{(1-\mu_L^*)} = R_P^{\frac{1-k}{k}} \tag{31}$$

Two curves obtained by solving the two previous equations are presented in Fig. (5). The first one is $\theta_L^*\times R_P$, whereas the other curve is $\mu_L^*\times R_P$. Roughly, the ideal cold mass fraction associated with the optimal COP_s falls between 0.55 for very low pressure ratios and 0.90 for a large pressure ratio ($R_P = 20$), having an increasing monatomic behavior with the increasing of the pressure ratio. On the other hand, the ideal optimal dimensionless cold temperature is located between 0.3 and 0.9, and the function displays a decreasing monatomic behavior with the increasing pressure ratio. One will not overemphasize if one recalls that the ideal optimum parameters for the R–H tube in the heat pump operating mode is promptly obtained by substituting the solutions μ_L^* and θ_L^* into Eqs. (2) and (6) to obtain μ_H^* and θ_H^*. All the above calculations were made for air, $k = 1.4$, and it will vary somewhat for different gases of a different heat capacities ratio.

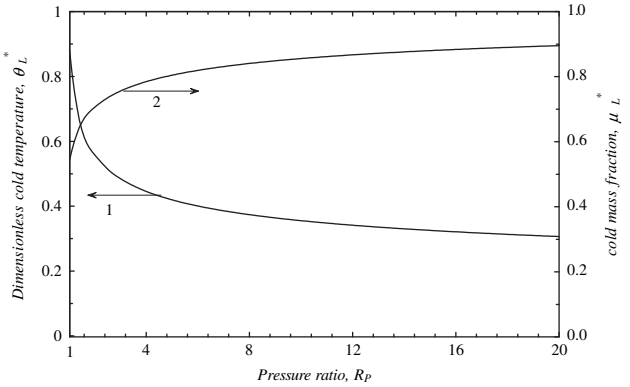

Fig. 5 – Optimal operating conditions where the COP_S is a maximum. Curve 1 is for the optimum dimensionless cold temperature, θ_L^*, versus pressure ratio, R_P. Curve 2 is for the optimum cold mass fraction, μ_L^*, versus pressure ratio, R_P. Air atmospheric ($k = 1.4$).

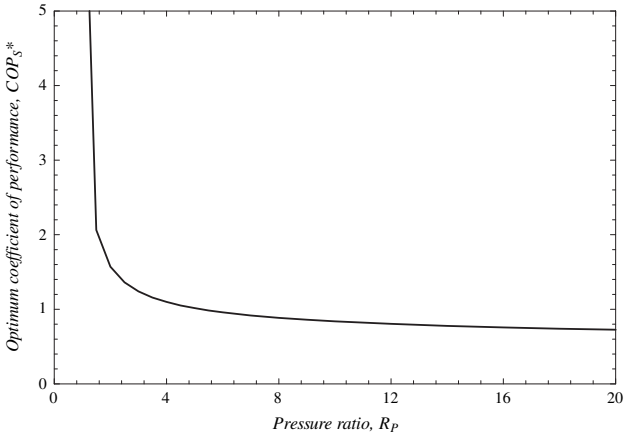

Fig. 6 – Optimal operating conditions where the COP_S is a maximum versus pressure ratio, R_P. Air atmospheric ($k = 1.4$).

The maximum or optimum COP_S^* associated with θ_L^* and μ_L^*as a function of the pressure ratio can be obtained by substituting those known values into the *COP* definition (Eq. (12)). A graph showing the COP_S^* dependency with the pressure ratio is shown in Fig. (6). As the pressure ratio approaches the unity, the COP_S^* goes to infinity which, of course, must be analyzed very carefully. At that limiting condition the compression power also goes to zero and, as the *COP* depends on reciprocal of the compression power, its value will become unbound. It is interesting to notice that, for air, the COP_S^* is greater than the unity for pressure ratios, R_P, within approximately the range just above 1 up to 3 and it slowly decreases monotonically for higher values of pressure ratios.

4. Comparison with some experimental data

Table 1 in Eiamsa-ard and Promvonge (2008)'s work presents a compilation of published experimental data from several researchers. Unfortunately, the dataset is not complete with all necessary information to carry out a full analysis. Nevertheless, their table was used in order to compare the present analysis with data obtained in laboratory for those available data (cold and hot temperature difference along with the cold mass fraction). The first 3 columns of Table 1 were directly extracted from Table 1 of their work. The first column refers to the data author and for any further reference details it is suggested to refer to their paper. The second column refers to the inlet pressure, P_0, and the third column displays the cold mass fraction, μ_L. Next two columns show the cold and hot temperature differences. In order to carry out the study, it was necessary to obtain the corresponding dimensionless temperatures and a test temperature had to be assumed, $T_0 = 298.15$ K (25°C), for switching from temperature differences to dimensionless temperatures. The corresponding dimensionless temperatures are shown in 6th and 7th columns.

After collecting experimental data, the first analysis one should perform is to check if the First Law of Thermodynamics is fulfilled. That can easily be accomplished by checking experimental data against either Eq. (6) or Eq. (7),

Table 1 – Experimental data collected from literature by Eiamsa-ard and Promvonge (2008). Only complete data are presented. The original data were reduced to variables according to the present work. It was assumed $T_0 = 298.15$ K (25 °C) and $P = 1$ atm.

Author[a]	P_0 (atm)	μ_L	ΔT_L (K)	ΔT_H (K)	θ_L	θ_H	*1st law* check	*COP* (actual)	COP_S (ideal)
Hilsh	11	0.23	53	140	0.822	1.470	1.32	0.060	0.329
Scheper	2	0.26	11.7	3.9	0.961	1.013	1.00	0.052	1.001
Scheller & Brown	6.1	0.506	23	15.6	0.923	1.052	0.99	0.076	0.783
Otten	8	0.43	50	40	0.832	1.134	1.00	0.121	0.631
Vennos	5.76	0.35	13	−1	0.956	0.997	0.98	0.031	0.618
Bruun	2	0.23	20	6	0.933	1.020	1.00	0.078	0.920
Stefhan et al.	6	0.3	38	78	0.873	1.262	1.14	0.075	0.537
Amitani et al.	3.06	0.4	19	15	0.936	1.050	1.00	0.080	0.947
Negm et al.	6	0.38	42	30	0.859	1.101	1.01	0.105	0.646
Ahlborn et al.	2.7	0.4	27	30	0.909	1.101	1.02	0.128	1.027
Promvonge and Eiamsa-ard	3.5	0.38	30	25	0.899	1.084	1.01	0.107	0.845
Aljuwayhel et al.	3	0.1	11	1.2	0.963	1.004	1.00	0.012	0.315

a For full reference, refer to Eiamsa-ard and Promvonge (2008).

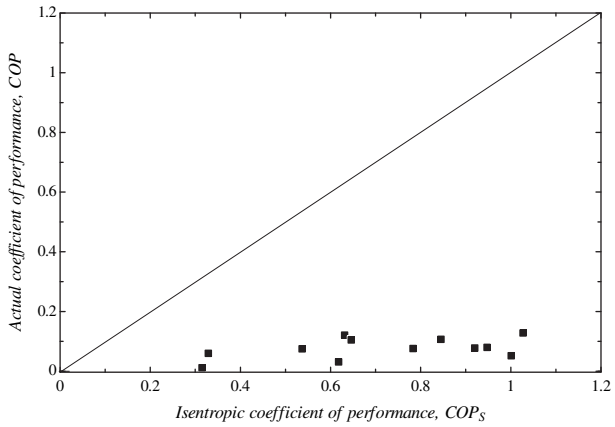

Fig. 7 – Comparison of actual COP and the corresponding isentropic or ideal COP_S for the experimental data presented in Table 1. For the experimental data it was assumed: air atmospheric ($k = 1.4$), $T_0 = 25$ °C and $P = 1$ atm (101.325 kPa).

given that they are equivalent. So, in order to verify the consistency of the experimental data base, the 8th column in Table 1 was obtained by substituting the set of experimental data (θ_L, θ_H, and μ_L) into Eq. (6). The fulfillment of First Law would lead to a unity. Of course, one may consider any small discrepancy due to the dependence of air the heat capacity with temperature. 9th column in Table 1 shows the corresponding experimental COP (actual) obtained from Eq. (12). It was assumed an environment pressure equals to $P_{atm} = 1$ atm (101.325 kPa), which may not be true for all of the collected data. Finally, the last column represents the corresponding COP_S (ideal) isentropic limit calculated according to Eq. (26) for each set of experimental data.

Fig. (7) shows a comparison of actual COP against the corresponding isentropic or ideal COP_S for the experimental data presented in Table 1 (last two columns). Ideally, experimental data points should cluster around the bottom side of the 45° straight line. However, there is a high data points concentration just about the low COP region, which is a clear indication that that most actual R–H tubes are highly irreversible devices, at least for those analyzed in this paper.

5. Discussions and conclusions

This paper analyzed the limiting operating conditions of an ideal Ranque–Hilsh tube operating in steady state. The first limit is set by the trivial solution in which the tube works as a simple adiabatic throttling device. No temperature variation between the inlet and outlet occurs and the COP is nil. The other limit is established by the Second Law of Thermodynamics as given by Eq. (21) or, alternatively, by Eq. (22). Any actual R–H tube operation is bound by those two limits.

Initially, the paper carried out independent analyses for a refrigeration operating mode and for a heat pump operating mode. Through out the study it was shown that the results are completely similar and they can alternate by simply selecting the set of independent variables of interest, i.e., cold mass fraction and cold temperature for refrigeration mode or hot mass fraction and hot temperature for heat pump mode. Therefore, it is not necessary to define a COP for each operating mode, as they are the identical and it can plainly be named as the ''COP of the R–H tube''.

An analytical equation for the cold temperature as a function of the cold mass fraction could be obtained from the hypothesis of ideal gas behavior with constant heat capacities. Eq. (21) presents such equation in an implicit form. Similarly, it is possible to obtain an equivalent equation for the hot temperature as a function of the hot mass fraction (Eq. (22)).

The graph of Fig. (2) indicates that very low temperatures are allowable by solving the conservation equations in an R–H tube if it could operate near the isentropic conditions. In fact, R–H tubes have been used for obtaining liquefied natural gas at cryogenic temperatures (Khodorkov et al., 2003; Kirillov, 2004). Conversely, high temperatures can also be obtained.

The analysis showed that there is an optimal or maximum COP for an ideal R–H tube operating at isentropic conditions as depicted in Fig. (4). In order to investigate that behavior further, it was carried out an analysis of that optimum condition. That was accomplished by applying the condition of maximum (Eq. (28)) to the Eq. (26). The curve in Fig. (6) shows the relationship between the maximum COP_S^* and the pressure ratio for air ($k = 1.4$). As shown in that curve, it is possible to obtain a COP_S greater than the unity for pressure ratios up to 3 for air.

The cold mass fraction corresponding to the ideal maximum COP_S^* for a large range of pressure ratios (from nearly 1 up to 20) falls within 0.55–0.90. Nimbalkar and Muller (2009) inform that measured optimum COP values for some previous tested devices were located between 0.5 and 0.7. Their work had an optimum COP for a mass cold fraction around 0.6.

Mass fractions have been used in this study as independent parameters (actually, only one of two mass fractions is independent). It is worthy to mention that the mass fraction (cold or hot one) is intimately and directly associated with the internal construction of an R–H tube. They can be established by selecting appropriate dimensions and shapes of area passages within the tube.

Analyses carried out on the COP have shown that actual R–H tubes are highly irreversible devices. The actual COP can be as low as 5% of the isentropic COP_S for the data analyzed in this paper, which opens up room for further work on optimization and proper internal orifices and flow passages design.

Finally, this paper did not speculate on the physical mechanisms that may occur inside an R–H tube, but rather the study concentrated only on an integral control volume approach using the laws of conservation. It is an open field for discussion to investigate further what are the dominating physical mechanisms that split the original fluid flow into hot and cold fluid streams. As a personal view, the author speculates that compressible phenomena should be responsible for the temperature separation within the tube. The Prandtl–Meyer process may occur just at the compressed air expansion at the inlet orifice exit section leading to a low temperature stream at the tube center line that would be driven to the cold end exit. Given the compressible flow nature, it is also

possible that complex shock waves would be accountable for raising the temperature to obtain the hot stream exit.

Acknowledgments

The author thanks CNPq for personal support. This work was concluded while the author was a short term visiting professor at Cethil-INSA de Lyon (France).

REFERENCES

Ahlborn, B.K., Gordon, J.M., 2000. The vortex tube as a classic thermodynamic refrigeration cycle. J. Appl. Phys. 88 (6), 3645–3653.

Aljuwayhel, N.F., Nellis, G.F., Klein, S.A., 2005. Parametric and internal study of vortex tube using a CFD model. Int. J. Refrigeration 28, 442–450.

Behera, U., Paul, P.J., Kasthurirengan, S., Karunanithi, R., Ram, S.N., Dinesh, K., Jacob, S., 2005. CFD analysis and experimental investigations towards optimizing the parameters of Ranque–Hilsh vortex tube. Int. J. Heat Mass Transfer 48, 1961–1973.

Deissler, R.G., Perlmutter, M., 1960. Analysis of the flow and energy separation in a vortex tube. Int. J. Heat Mass Trasfer 1, 73–191.

Dincer, K., Tasdemir, S., Baskaya, S., Uysal, B.Z., 2008. Modeling of the effects of length to diameter ratio and nozzle number on the performance of counterflow Ranque–Hilsch vortex tubes using artificial neural networks. Appl. Therm. Eng. 28, 2380–2390.

Eiamsa-ard, S., Promvonge, P., 2008. Review of Ranque–Hilsh effects in vortex tubes. Renew. Sust. Energy Rev. 12, 1822–1842.

Fulton, C.D., 1950. Ranque tube. J. ASRE Refrig. Eng., 473–479.

Gao, C.M., Bosschaart, K.J., Zeegers, J.C.H., de Waele, A.T.A.M., 2005. Experimental study on a simple Ranque–Hilsch vortex tube. Cryogenics 45, 173–183.

Hartnett, J.P., Eckert, E.R.G., 1957. Experimental study of the velocity and temperature distribution in a high velocity vortex tube flow. Trans. ASME 79, 751–758.

Hilsch, R., 1946. Die Expansion von Gasen im Zentrifugalfeld als Kälteprozess. Zeitung für Naturforschung 1, 208–214.

Khodorkov, I.L., Poshernev, N.V., Zhidkov, M.A., 2003. The vortex tube – a universal device for heating, cooling, cleaning, and drying gases and separating gas mixtures. Chem. Pet. Eng. 39, 409–415.

Kirillov, N.G., 2004. Analysis of modern natural gas liquefaction technologies. Chem. Pet. Eng. 40, 310–315.

Lay, J.E., 1959. An experimental and analytical study of vortex flow and temperature separation by superposing of spira and axial flow, part 1 an part 2. ASME J. Heat Transf 81, 316–317.

Lewins, J., Bejan, A., 1999. Vortex tube optimization theory. Energy 24, 931–943.

Martynovskii, V.S., Alekseev, V.P., 1957. Investigation of the vortex thermal separation effect for gases and vapors. Sov. Phys. Tech. Phys., 2233–2243.

Metenin, V.I., 1961. Investigations of vortex tube type compressed air separators. Sov. Phys. Tech. Phys. 15, 1025–1032.

Nimbalkar, S.U., Muller, M.R., 2009. An experimental investigation of the optimum geometry for the cold end orifice of a vortex tube. Appl. Therm. Eng. 29, 509–514.

Pengelley, C.D., 1957. Flow in a viscous vortex. J. Appl. Phys. 28, 86–92.

Ranque, G.W., 1933. Expèriences sur la dètente giratoire avec productions simultanées d'un échappement d'air chaud et d'un échappement d'air froid. Le J. De Physique 4, 112–115.

Reynolds, A.J., 1964. A note on vortex-tube flows. J. Fluid Mech. 14, 18–20.

Saidi, M.H., Valipour, M.S., 2003. Experimental modeling of vortex tube refrigerator. Appl. Therm. Eng. 23, 1971–1980.

Scheperjr., G.W., 1951. The vortex tube internal flow data and a heat transfer theory. J. ASRE Refrig. Eng. 59, 985–989.

Takahama, H., 1965. Studies on vortex tubes. Bull. JMSE 8 (31), 433–440.